CHAPTER IV
NANO-STRUCTURED CHITOSAN FOR ALLERGEN DELIVERY SYSTEM

Abstract

Nanoparticulate LCS-Phe-mPEG obtained from the conjugation of phenylalanine (Phe) and poly(ethylene glycol)methyl ether terminated with a carboxyl group (mPEG-COOH) onto low molecular weight chitosan is proposed. The structural characterization confirmed by FTIR at 1670 to 1630, 1551 to 1534, and 750 cm^{-1} for amide I, amide II, and the benzene ring of phenylalanine, respectively, and by ^1H NMR at 7.36 to 7.24 and 2.63 to 2.48 ppm for C_6H_5 of phenylalanine and $COCH_2CH_2CO$ of mPEG, respectively, indicates the successful reaction. Compound **2** exhibits the size of 150-250 nm in solution state, as evaluated by dynamic light scattering (DLS), and 50-60 nm in spherical shape in dry state as observed by TEM. A preliminary study of allergen entrapment done by simply mixing nanoparticles with the crude allergen solution shows a UV-Vis absorption at 595 nm, indicating the successful allergen incorporation in the nanoparticulate LCS-Phe-mPEG.

Keywords: Chitosan, Nanoparticle, Adjuvant, Allergen delivery system

4.1 Introduction

Allergy is one of prevalent diseases caused by over sensitization in immune process which still needs an effective treatment. Although avoidance of the allergen exposure is the most important matter, several treatments such as drug therapy, allergen immunotherapy are the known clinical cure.[1] Recently, allergen delivery system has received much attention since it is a fundamental approach which concerns the addition of a series of allergen combining with adjuvants to increase allergen immune response by balancing T-helper cells 1 and 2.[2]

Chitosan is an aminopolysaccharide which known for the bioactivity, biocompatibility and biodegradability. Up to present, there are many reports related to the possibility to use chitosan in biomedical and pharmaceutical areas. For allergen delivery system, chitosan was reported as an adjuvant[3] to enhance the immune response of the cells. The fact that chitosan can be modified to various derivatives, the development of chemical structure of chitosan to incorporate allergen into chitosan is a good strategy to achiever chitosan allergen delivery system.

Recently, the progress in analytical instrument has led us to a better understanding of the polymer morphologies and their properties and performances in nanometer level. This also brings us to an understanding of the relationship between the primary chemical structures and the consequent nanometer scaled morphologies and properties. There are many reports related to the challenges in unique molecular designs which prove us the nanoparticles formation with specific morphologies in terms of nanorods[4], nanospheres[5], micelles[6], vesicles[7], etc. It comes to an expectation that those nano-sized materials are potential materials for drug carriers, gene deliveries, and molecular biology related therapies.[8]

In the case of nanospheres, several reports showed how various materials are potential for drug delivery and targeting. In terms of allergen delivery system, nanospheres can be expected to provide a sustained release of the allergen with effectiveness and efficacy at cell level.

On this viewpoint, currently, we succeed in preparing chitosan nanoparticles by simply introducing hydrophobic and hydrophilic groups onto the chains.[9] In separate work, we also found that chitosan formed a complex with

hydroxybenzotriazole (CS-HOBt) which allowed water solubility.[10] The CS-HOBt allowed us to carry out the conjugating reaction via the homogeneous system with the use of water soluble conjugating agent.

The present work is another step to extend the nanospherical chitosan for a concrete molecular design and synthesis for a practical application of allergen delivery system. Therefore, an important point is about how to functionalize chitosan with biomolecules to achieve biocompatible nanoparticles with structures and/or morphologies of which allergen incorporation is possible. Herein, we propose a model nanoparticulate chitosan based on the conjugation of amino acid molecules and polyethylene glycol via a simple conjugation reactions.

4.2 Experimental Section

4.2.1 Materials

Low molecular weight chitosan (LCS) was a gift from Chitin Research Center, Chulalongkorn University. 1-Hydroxybenzotriazole monohydrate ($HOBt{\cdot}H_2O$) and 1-ethyl-3-(3-dimethylaminopropyl-carbodiimide) hydrochloride (EDC·HCl) were purchased from Wako Pure Chemical Industries Co., Ltd., Japan. DL-Phenylalanine (Phe) and succinic anhydride were obtained from Fluka Chemika, Switzerland. Poly(ethylene glycol)methyl ether (mPEG, M_n 5000 Da) was the product from Sigma-Aldrich, Inc., USA. Allergen extract (*D.pteronyssius*) was purchased from ALK ABELLÓ, USA. Methanol was from the product of Carlo Erba reagent, Italy. All chemicals were used as received without further purification.

4.2.2 Instruments and Equipment

Qualitative Fourier transform infrared (FT-IR) spectra were recorded by a Bruker Equinox 55/S with 32 scans at resolution of 4 cm^{-1} in a frequency range of 4000-650 cm^{-1} using a deuterated triglycinesulfate detector (DTGS) with a specific detectivity, D*, of 1×10^9 cm Hz ½ w^{-1}. Degree of substitution was determined by using a Bruker Ultrashield 500 Plus NMR system. Concentration of allergen was determined by a Shimadzu UV-Vis spectrophotometer (UV-1800). The Z-average diameter of samples was determined by a Malvern Zetasizer Nano Series (Malvern

Instruments Ltd.) with a detection angle of 173°, dynamic light scattering (DLS). Transmission electron micrographs were observed by an H-7650 Hitachi transmission electron microscope at 100 kV. A Perkin Elmer Pyris Diamond thermogravimetric /differential thermogravimetry analyzer (TGA/DTG) was used with a N_2 flow and a heating rate of 10 °C/min from 30-600 °C. Wide angle X-ray diffraction patterns (WAXD) were obtained from a Rigaku D/MAX 2200 X-Ray wide angle diffractometer using a scan range 5°-90° 2θ with a scan step of 0.05° 2θ and a scan speed of 5° 2θ /min.

4.2.3 Poly(ethylene glycol)Methyl Ether Terminated with a Carboxyl Group (mPEG-COOH)

The reaction was carried out as reported by Yoksan *et al.* In brief, mPEG (M_n = 5000 Da, 3 g) was reacted with succinic anhydride (0.06 g, 1 mole equivalent to mPEG) at 60 °C overnight in the presence of a catalytic amount of pyridine. The solution obtained was concentrated and precipitated in diethyl ether before drying in vacuo to obtain mPEG-COOH.

FT-IR (ZnSe, cm^{-1}): 3503 (OH), 2864 (C-H stretching), 1733 (C=O), and 1112 (C-O-C).

*4.2.4 Phe and mPEG conjugated Chitosan, **2***

LCS (0.1 g, 1 mole) was vigorously stirred with HOBt (0.08 g, 1 mole equivalent to LCS) in deionized water (20 ml) at ambient temperature until the solution became clear. LCS-HOBt solution was mixed with Phe (0.10 g, 1 mole equivalent to LCS) and mPEG-COOH (2.95 g, 0.1 mole equivalent to LCS) in deionized water 10 ml followed by adding EDC (0.11g, 1 mole equivalent to LCS) into the solution. The homogeneous solution was carried out at ambient temperature overnight. The crude product was dialyzed, lyophilized, washed with methanol, and dried under vacuum to obtain LCS-Phe-mPEG, **2**. Other reactions with different mole ratios of Phe (0.5, 1.0, 1.5, 2.0, 2.5, and 3.0 equivalent to LCS) and mPEG-COOH (0, 0.1, 0.2, 0.3, 0.4, and 0.5 equivalent to LCS) were also prepared in the same procedures as **2**.

4.2.5 Allergen Incorporation

The incorporation of allergen was carried out in deionized water. A concentration of chitosan solution (1 mg/ml) and allergen (21.7μg/ml) was mixed and vigorously stirred for a minute at ambient temperature. The concentration of entrapped allergen was calculated from a difference between concentration of loading allergen and concentration of allergen in supernatants by UV-Vis spectroscopy (Bradford protein assay at a UV-Vis wavelength at 595 nm) and HPLC technique.

4.3 Result and Discussion

4.3.1 Structural Characterization

As chitosan used in the present work was obtained from the chitosan treated by chitosanase enzyme from *Bacillus*. sp.PP8, the molecular weight and %DD were identified in the first step. It was found that the molecular weight was 15000 (PDI = 1.9) and the %DD was 71 as identified by GPC and NMR, respectively. The overview of molecular design and synthesis are summarized in **Scheme 4.1**.

Scheme 4.1

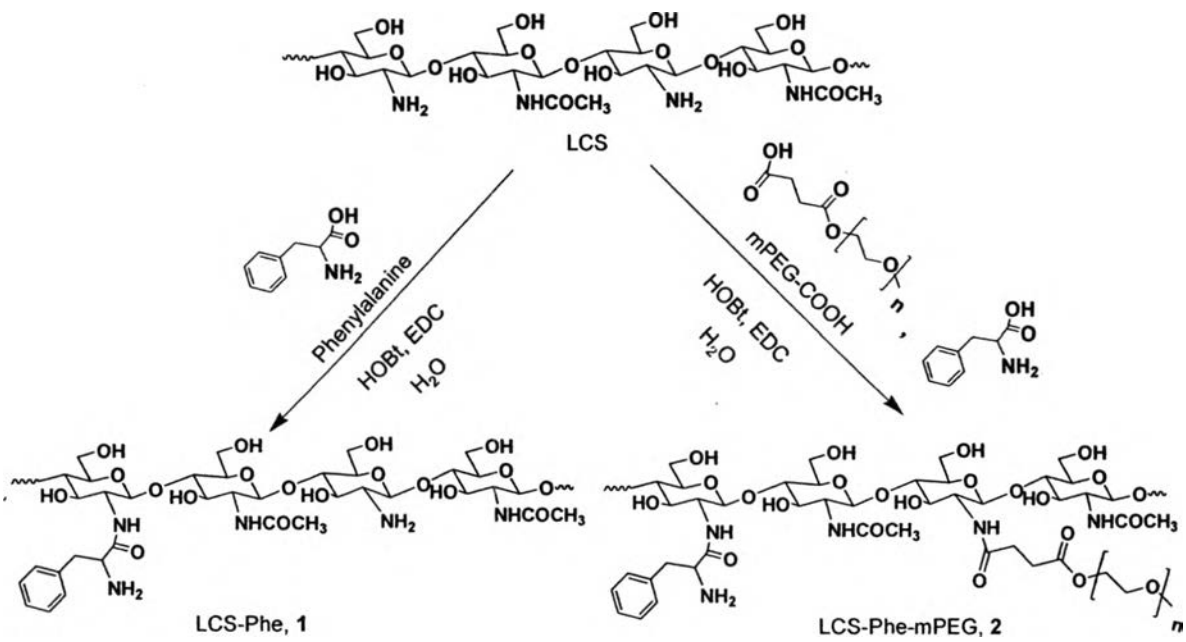

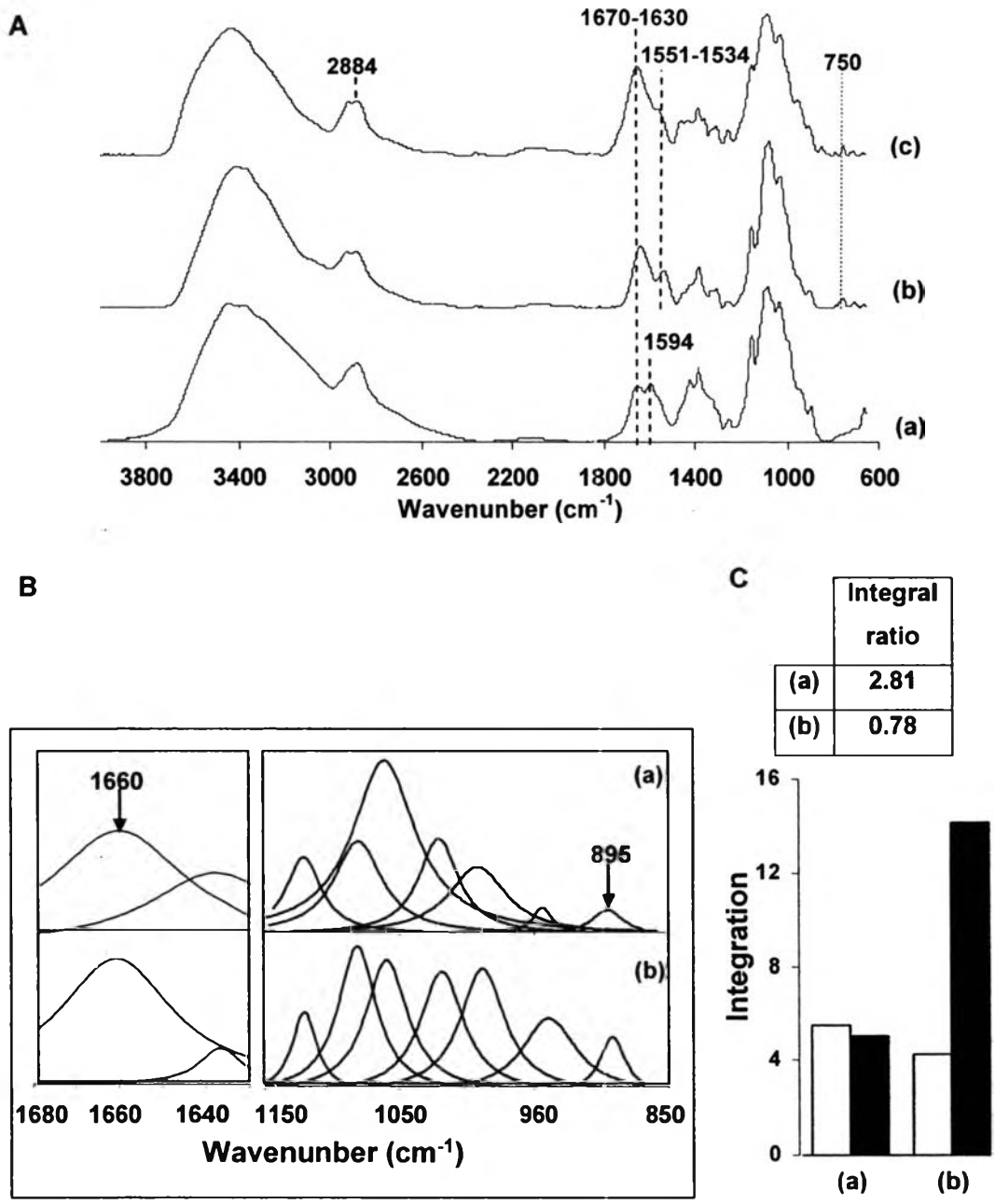

Figure 4.1 (A) FT-IR spectra of (a) LCS, (b) **1**, and (c) **2**; (B) curve fitting of (a) LCS and (b) **1**; and (C) integration of A_{895} (column □), A_{1660} (column ■), and the integral ratio obtained.

Compounds **1** and **2** (**Figure 4.1A**) show the changes in FT-IR spectra after LCS was conjugated with Phe and mPEG-COOH. For example, the peaks at 1660

cm^{-1} and 750 cm^{-1} for amide linkage and benzene ring of Phe are observed. This implies the structure of **2**. Here, to quantitatively analyze an appropriate molar ratio of phenylalanine, the FT-IR curve fitting (**Figure 4.1B**) based on an integral ratio between the peak at 1660 cm^{-1}(amide I) and the internal peak at 895 cm^{-1} (C-O-C of pyranose ring) was carried out. **Figure 4.1C** shows an increase of integral ratio of **1** after Phe was conjugated. The conjugation of mPEG-COOH can be confirmed from the significant peak at 2884 cm^{-1} referring to CH stretching of ethylene glycol unit (**Figure 4.1A**). It is important to note that the conjugation is also possible at C-6 (OH) group, however, **Figure 4.1A (b)** and **Figure 4.1A (c)** do not show any ester peak which leads to the structure as shown in **Scheme 4.1**.

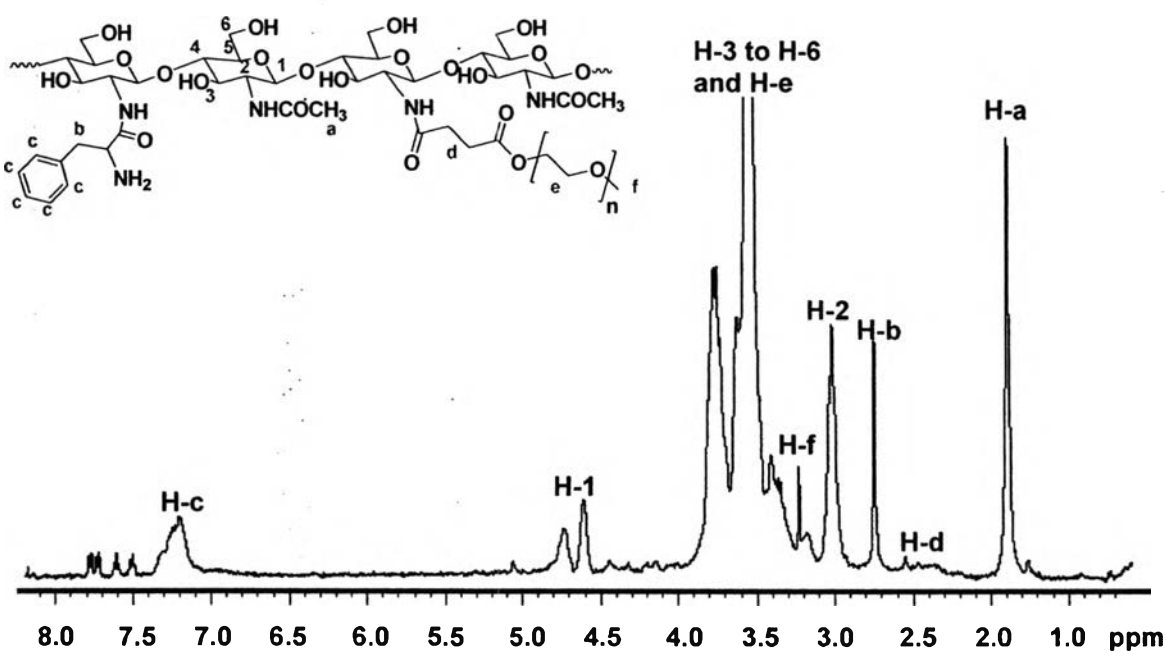

Figure 4.2 ^{1}H NMR spectrum of **2** in 2%CD_3COOD/D_2O.

^{1}H NMR (**Figure 4.2**) at room temperature also confirms the conjugation of Phe and mPEG with LCS. Compound **2** shows new chemical shifts at 7.36-7.24 ppm for $C_6\mathbf{H}_5$ (H-c) of Phe, at 2.63-2.48 for $COC\mathbf{H}_2C\mathbf{H}_2CO$ (H-d), and at 3.28 ppm for $C\mathbf{H}_3$ (H-f) of mPEG. Degree of substitution was calculated based on integrations of H-c and H-d with an integration of H-2 as internal standard. It was found that %DS of Phe for **1** and **2** were 10.60 and 11.60, respectively, while %DS of mPEG-COOH for **2** was 7.75 (see Appendix B).

4.3.2 Evaluation of Thermal Stability and Packing Structure

The packing structures of **1** and **2** were followed by XRD patterns. Generally, chitosan shows two peaks at 11° 2θ and 20° 2θ (**Figure 4.3 (a)**). After conjugating with Phe and mPEG-COOH, a shift of peak positions and broadness of peaks are observed (**Figures 4.3 (b)** and **4.3 (c)**). This might be due to the destruction of native chitosan packing structure after Phe and mPEG were successfully conjugated.

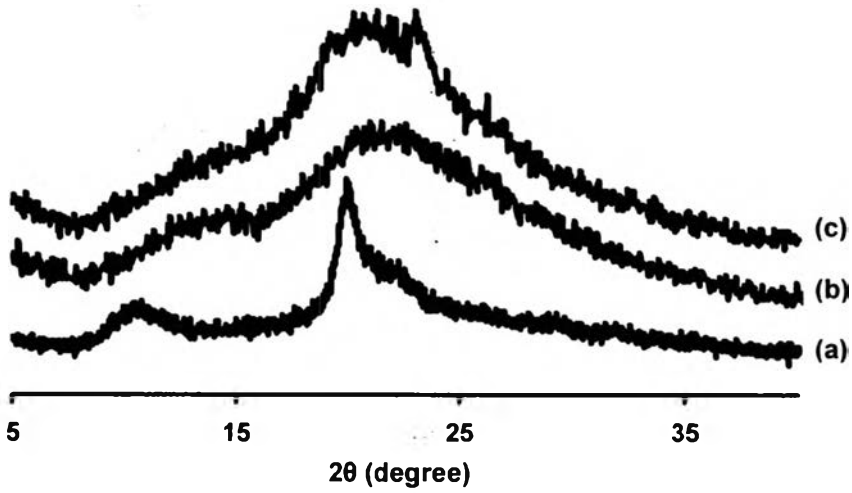

Figure 4.3 XRD patterns of (a) LCS, (b) **1**, and (c) **2**.

Differential thermogravimetric analysis (DTG) was used to trace the thermal stability after conjugation of Phe and mPEG onto LCS. **Figure 4.4 (a)** shows the degradation temperature (T_d) of LCS at 295 °C whereas that of **1** (**Figure 4.4 (b)**) is much lower and appears at 247 °C. This reflects the bulkiness of Phe obstructing the chain packing. The result is supported by the XRD pattern observed in **Figure 4.3 (b)** which the peak are significantly broad. For **2** (**Figure 4.4 (c)**), there are two degradation steps at 256 °C and 391 °C. The degradation peaks are relevant to those of Phe (**Figure 4.4 (d)**) and mPEG-COOH (**Figure 4.4 (e)**). It is important to note that the degradation temperature of chitosan at 295 °C was not observed after conjugating with mPEG and Phe. This also implies that the chain packing of chitosan was changed after the conjugation and the degradation peaks reflect the effect of bulky groups in packing structure.

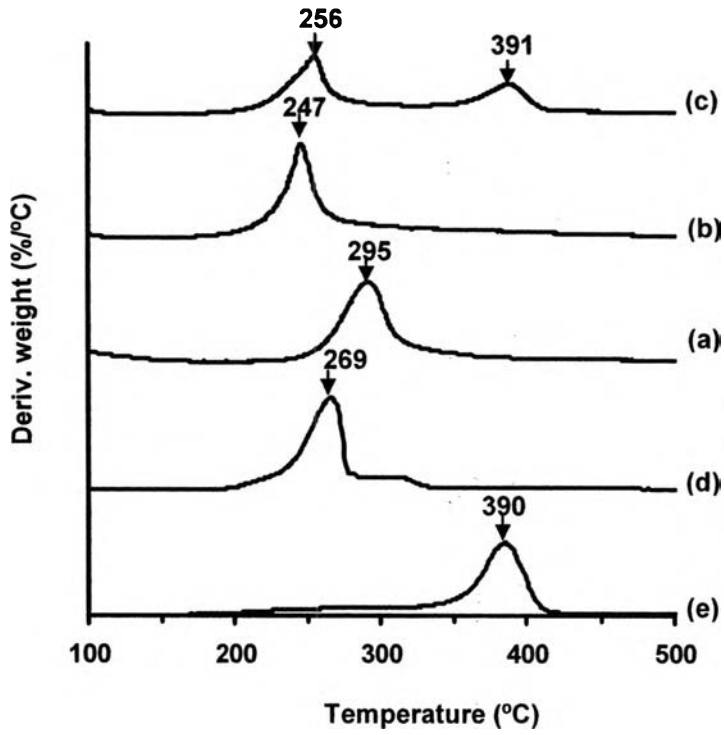

Figure 4.4 DTG thermograms of (a) LCS, (b) **1**, (c) **2**, (d) Phe, and (e) mPEG-COOH.

4.3.3 Evaluation of Size and Morphology

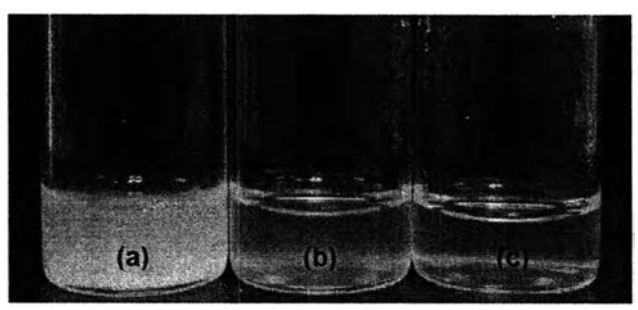

Figure 4.5 Appearances of (a) LCS, (b) **1**, and (c) **2** dispersed in deionized water (concentration 1.5 mg/ml).

In general, chitosan and almost all derivatives are insoluble in water. In our case, **2** gives a colloidal solution and was maintained for 3 days (**Figure 4.5**). This

phenomenon might come from the fact that the conjugation of Phe and mPEG was successful. As a result, the substituted molecules might disturb chitosan aggregation. In addition, there might be some hydrogen bonds between water and oxygen atoms of mPEG. The average diameter sizes of LCS, **1**, and **2** in solution state were determined by dynamic light scattering technique. **Figure 4.6** shows diameter size of 939, 625, and 206 nm, for LCS, **1**, and **2**, respectively. The average diameter size of LCS-Phe is smaller than that of LCS which implies hydrophobic-hydrophobic interaction of the conjugated Phe. The average diameter size of **2** is smaller than that of **1** implies the role of hydrophilic part from mPEG.

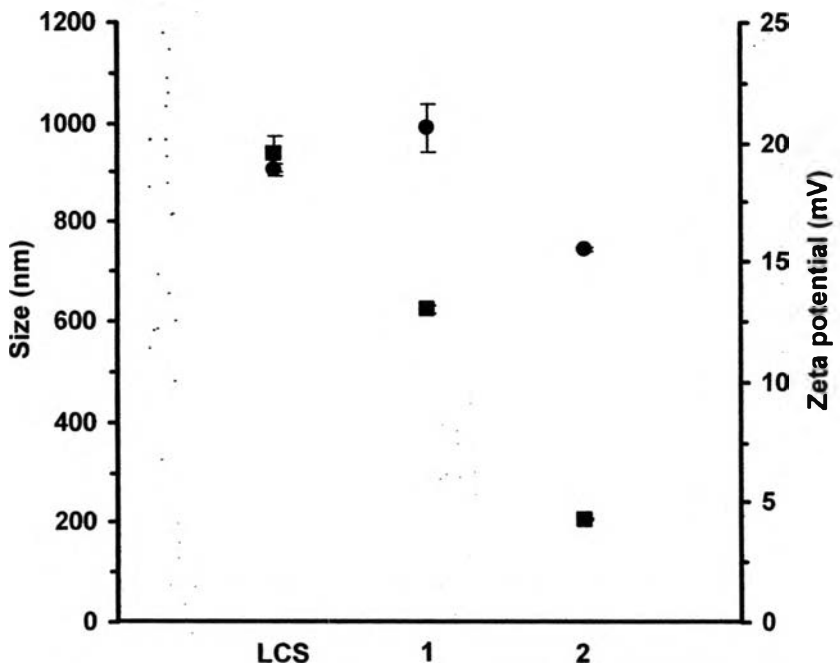

Figure 4.6 Size (■), and zeta potential (●) of (a) LCS, (b) **1**, and (c) **2** dispersed in deionized water (1.5 mg/ml). Results are means ± SD (n=3).

TEM was applied to determine an average diameter size in solid state. Compound **1** shows the size of ~600 nm (**Figure 4.7 (a)**) which is relevant to the DLS result. In the case of **2**, an individual particle is clearly observed which is in the size of ~50 nm (**Figure 4.7 (b)**). The significantly small size and the individual particles confirm how **2** is well dispersed and rarely aggregates among each other.

It is also important to investigate the surface charge which directly relates to drug incorporation. **Figure 4.6** also shows the zeta potential of LCS, **1**, and **2** to be ~ 15-20 mV in positive charge in deionized water.

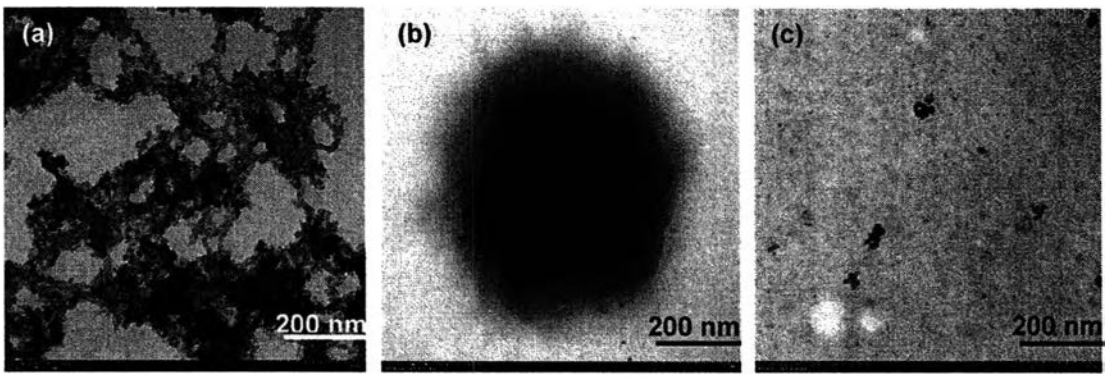

Figure 4.7 TEM micrographs of (a) LCS, (b) **1**, and (c) **2** (20,000× magnification).

4.3.4 Factors controlled Nanospherical Size

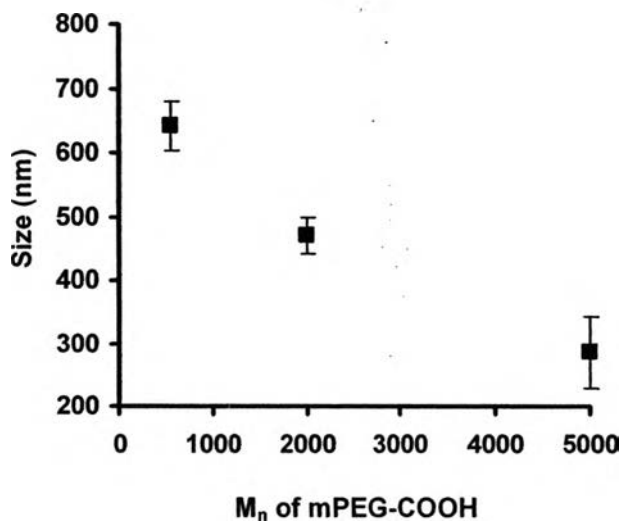

Figure 4.8 Particle size of **2** dispersed in deionized water (1.5 mg/ml). Results are means ± SD (n=3).

As shown in 4.3.3, evaluate size and morphology above, **2** gives the smallest size which may be appropriate for tissue penetration. Thus, **2** was collected to study

factors related to the changes of particle size (determined by DLS) such as M_n of mPEG-COOH, %DS of mPEG-COOH, and %DS of Phe.

When M_n of mPEG-COOH was varied for 550, 2000, and 5000 the particle size decreases as M_n of mPEG-COOH is increased (**Figure 4.8**). This might be due to the difference of surface energy (ΔE) between the surface energy at LCS chain attached mPEG (E_1) and that at LCS chain attached Phe (E_2). **Scheme 4.2** shows the effect of mPEG-COOH in shrinking the nanoparticle size.

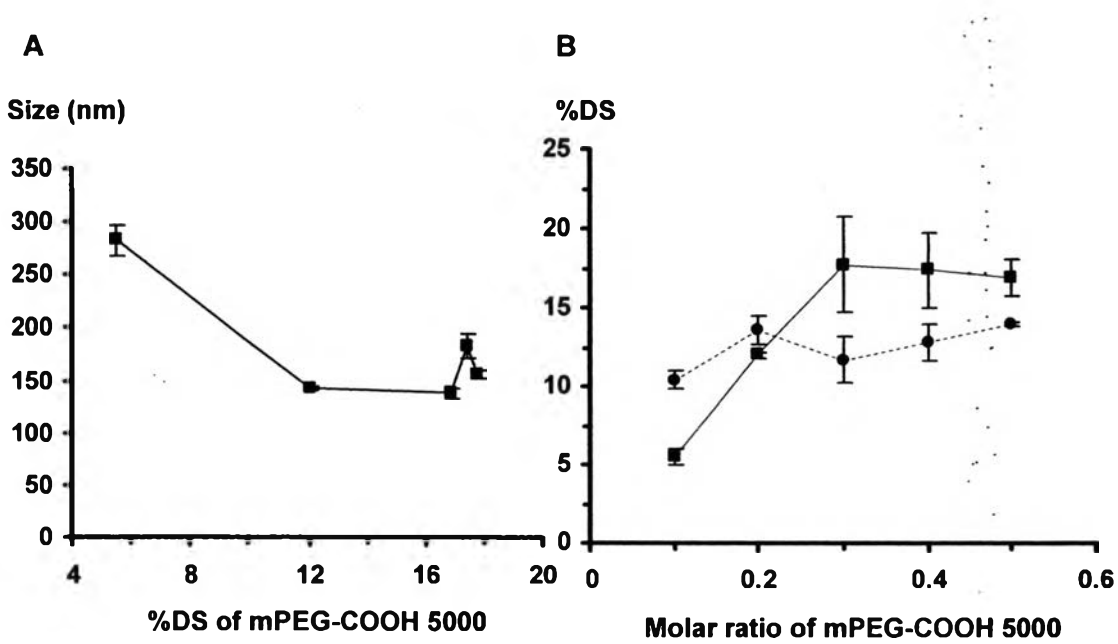

Figure 4.9 (A) Nanoparticle size of **2** dispersed in deionized water (1.5 mg/ml). Results are means ± SD (n=3); and (B) %DS of mPEG-COOH (■), and Phe (●).

Here, mPEG-COOH with M_n 5000 Dalton was studied in more details. **Figure 4.9A** shows a relationship between %DS of mPEG-COOH 5000 and particle size. The particle size decreases as %DS of mPEG-COOH 5000 is increased. This also confirms the significant hydrophilicity initiates the shrinking of nanoparticles as discussed on the viewpoint of surface tension. It comes to the question about the factors to control %DS of mPEG-COOH 5000. Here, the molar ratio of mPEG-COOH 5000 was varied. **Figure 4.9B** shows that, at a constant %DS of Phe, when molar ratio of mPEG-COOH 5000 is increased, %DS of mPEG-COOH 5000 increases and becomes constant at the molar ratio of mPEG-COOH to LCS of 0.3. It

can be concluded that molar ratio of mPEG-COOH 5000 is one of the factors to control the %DS of mPEG-COOH 5000 and as a consequent, the particle size.

Scheme 4.2

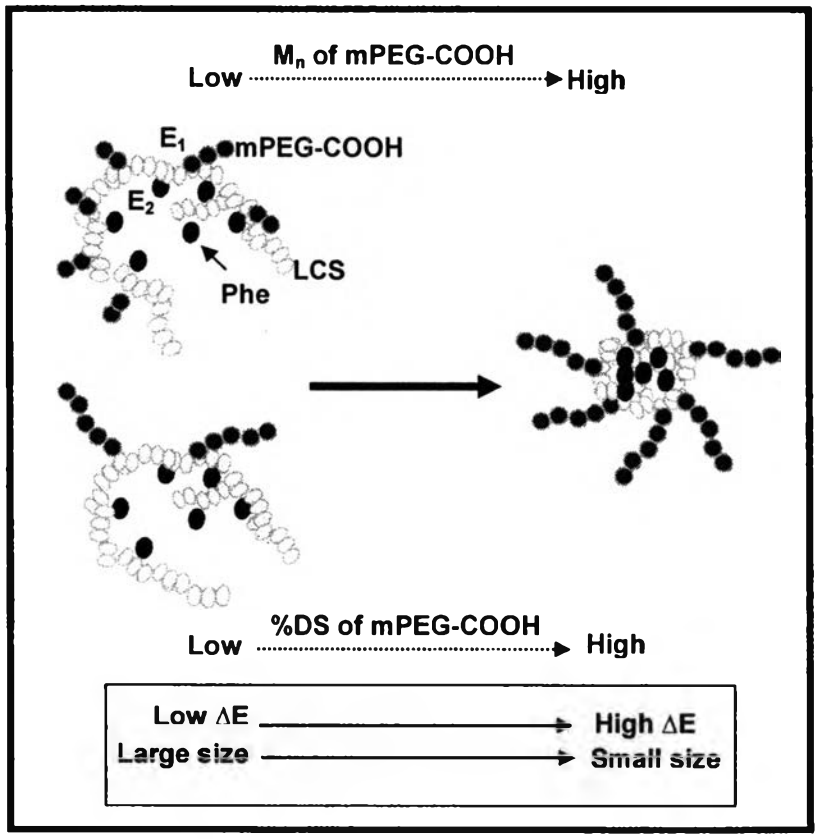

In similar, the factors to control %DS of Phe were studied. **Figure 4.10** shows how %DS of Phe is depending on the Phe content in the reaction. It is clear that although the molar ratio of Phe is increased, %DS of Phe becomes constant at around 10 to 14. It is important to note that when the molar ratio of Phe is increased, the %DS of mPEG-COOH 5000 decreased (**Figure 4.10A**) and at the same time the size is decreased (**Figure 4.10B**).

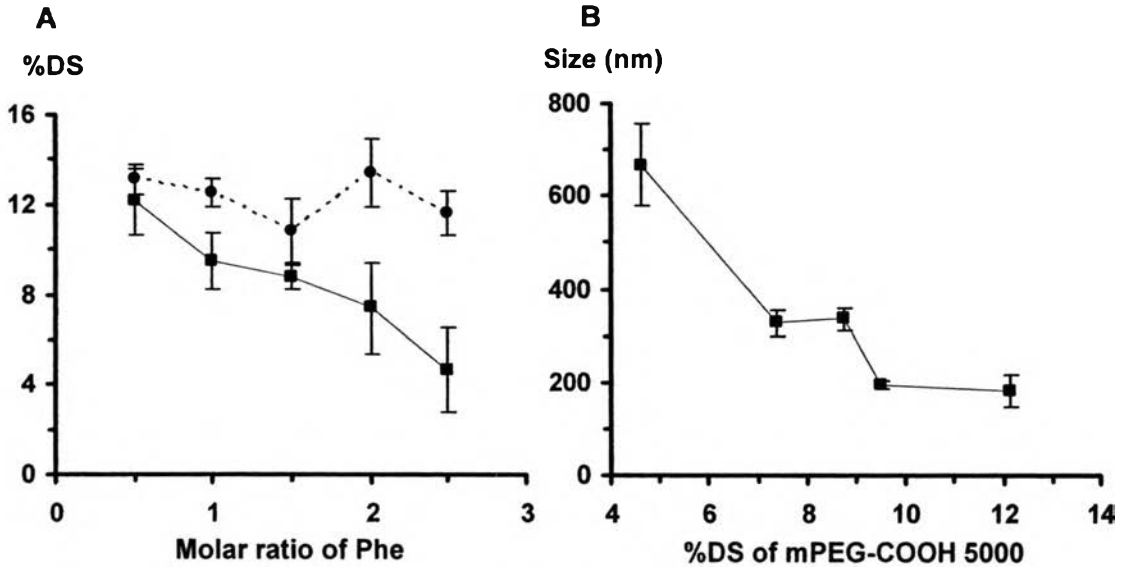

Figure 4.10 (A) %DS of mPEG-COOH (■), and Phe (●); and (B) nanoparticle size of **2** dispersed in deionized water (1.5 mg/ml). Results are means ± SD (n=3).

4.3.5 Allergen Incorporation

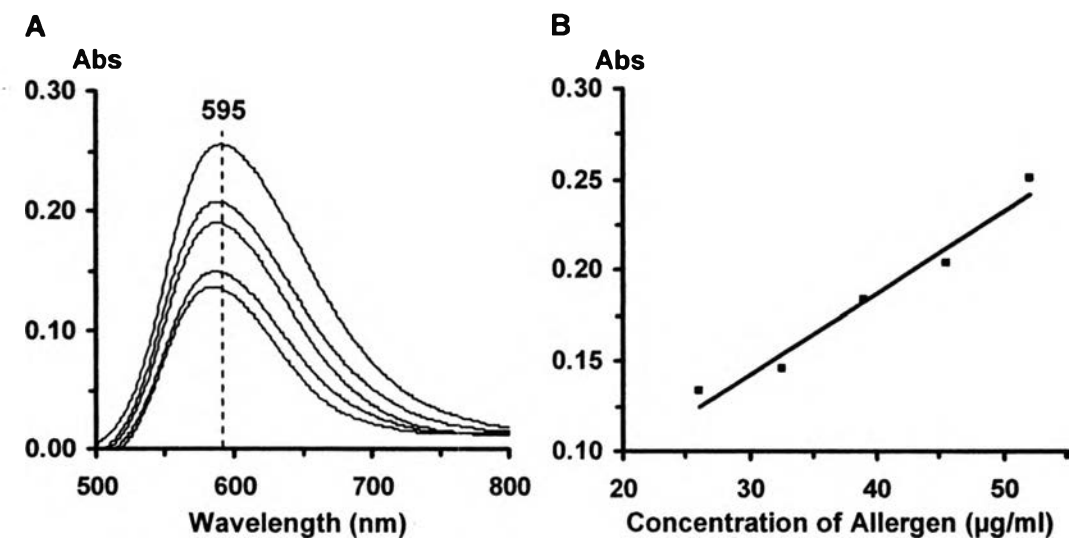

Figure 4.11 (A) UV-vis spectra of allergen with dye; and (B) allergen standard curve ($y=0.0045x + 0.0068$, $R^2 = 0.966$).

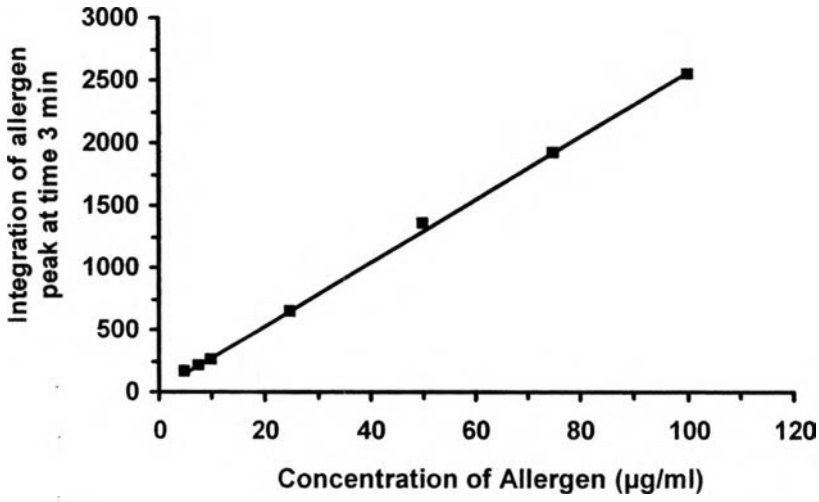

Figure 4.12 Allergen standard curve by HPLC ($y = 25.354x + 24.218$, $R^2 = 0.999$).

Table 4.1 Content of allergen in LCS, LCS (added with EDC), **2**, and **2** with EDC

Compound (loaded with allergen solution)	Content of entrapped allergen (%)	
	HPLC	UV-Vis spectroscopy
LCS	10.69 ± 0.80	34.19 ± 0.40
LCS (added with EDC)	8.94 ± 0.92	19.72 ± 1.48
2	2.70 ± 0.44	17.14 ± 2.58
2 with EDC	3.30 ± 0.63	17.34 ± 3.77

Allergen entrapment was carried out by using Bradford protein assay. Based on the binding of protein to Coomassive® Brilliant Blue dye, the protein amount can be traced by using UV-Vis spectrum at 595 nm. **Figure 4.11A** shows maximum absorbance in varied concentration of allergen. **Figure 4.11B** shows a standard curve of allergen solutions. From the standard curve, the allergen concentration of unknown sample can be evaluated. Here, the concentration of entrapped allergen in compound **2**, calculated from a difference between concentration of loading allergen and concentration of allergen in supernatants, was focused. The concentration of entrapped allergen in compound **2** was found to be 17.14 ± 2.58% indicating a successful allergen incorporation. Furthermore, HPLC technique was also used to

determine the concentration of entrapped allergen based on allergen standard curve (**Figure 4.12**). **Table 4.1** shows some values of % entrapped allergen for each sample in two techniques. Although these two techniques show quite different percent entrapped allergen, these values were changed in the same trend. In other words, the results support the allergen incorporation.

Figure 4.13 shows the morphology and size of entrapped allergen in **2**. It was found that there are 2 types of morphologies. One is spherical shape with size around ~ 250 nm (**Figure 4.13** (**a**)) which is bigger than **2** (**Figure 4.7** (**c**)). This might be due to allergen incorporation. **Figure 4.13** (**b**) also shows another type of the particles of **2** appearing as dark dots distributed in and out of allergen which appears to be network structure. In order to clarify the allergen entrapment, other related techniques, such as fluorescence labeling, are needed. However, the changes in morphology and size imply the possible allergen entrapment.

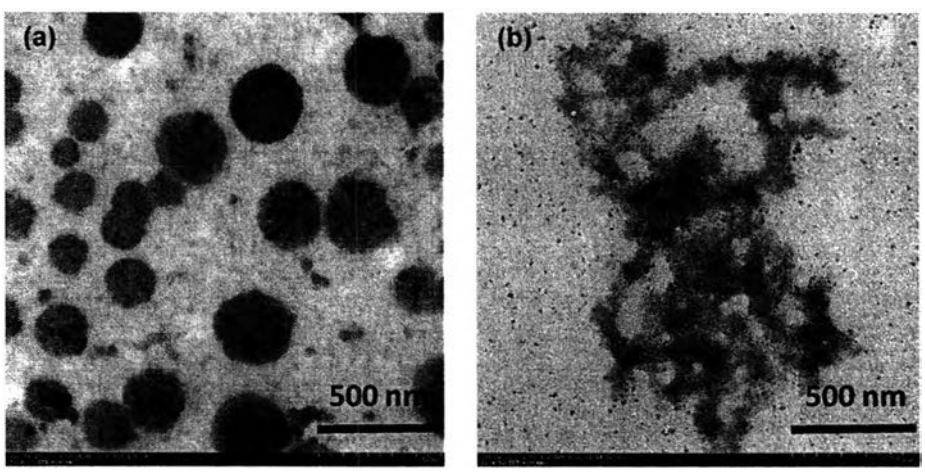

Figure 4.13 TEM micrographs of entrapped allergen in **2** (a) 10,000× magnification, and (b) 10,000× magnification.

4.4 Conclusions

Nano-structured chitosan was successfully prepared by introducing hydrophobic (Phe) and hydrophilic (mPEG-COOH) groups on low molecular weight chitosan chain via the water-soluble conjugated reaction. The compound obtained showed the %DS of Phe and mPEG ~10% with size ~150-250 nm in the solution

state and a spherical shape for ~50 nm in the dry state. The allergen entrapment was about ~20% by UV-Vis spectroscopy and ~ 3% by HPLC.

4.5 Acknowledgments

The author acknowledges the scholarship from TGIST (Thailand Graduate Institute of Science and Technology) and the Center for Petroleum, Petrochemicals and Advanced Materials, Chulalongkorn University. The author would like to extend their appreciation to Chulalongkorn University Centenary Academic Development Project, Chitin Research Center (Chulalongkorn University), and the Hitachi-High Technology Co., Ltd., Japan for TEM analysis.

4.6 References

1. **Rolland, J.M., Gardner, L.M., and O'Hehir, R.E.** (2009). Pharmacol. Ther. 121, 273–284.
2. **Huggins, J.L. and Looney, R.J.** (2004). Am. Fam. Physician. 70, 689-696.
3. **Schöll, I., Boltz-nitulescu, G., and Jensen-Jarolim, E.** (2005). J. Conrel. 104, 1-27.
4. **Cao, G. and Liu, D.** (2008). Adv. Colloid Interface Sci. 136, 45-46.
5. **Kataoka, K. and Nishiyama, N.** (2006). Pharmacol. Ther. 112, 630-648.
6. **Gaucher, G., Dufresne, M., Sant, V.P., Kang, N., Maysinger, D., and Lerous, J.** (2005). J. Controlled Release. 109, 169-188.
7. **Wiesman, Z., Dom, N.B., Sharvit, E., Grinberg, S., Linder, C. Heldman, E., and Zacca, M.** (2007). J. Biotechnol. 130, 85-94.
8. **Davda, J. De, S. Zhou, W., and Labhasetwar, V.** (2001). Biomedical Polymers and Polymer Therapeutics. pp 19-31. Plenum Publishers, New York.
9. **Yoksan, R., Akashi, M., Hiwatari, K.I., and Chirachanchai, S.** (2003). Biopolymers. 69, 386-390.
10. **Fangkangwanwong, J., Akashi, M., Kida, T., and Chirachanchai, S.** (2006). Macromol. Rapid Commun. 27, 1039-1046.